Electrical properties and the determination of interface state density from I−V, C−f and G−f measurements in Ir/Ru/n-InGaN Schottky barrier diode

© R. Padma, V. Rajagopal Reddy

Department of Physics, Sri Venkateswara University,
Tirupati-517 502, India
E-mail: reddy_vrg@rediffmail.com

The electrical properties of the Ir/Ru Schottky contacts on n-InGaN have been investigated by current-voltage $(I−V)$, capacitance-voltage $(C−V)$, capacitance-frequency $(C−f)$ and conductance-frequency $(G−f)$ measurements. The obtained mean barrier height and ideality factor from $I−V$ are 0.61 eV and 1.89. The built-in potential, doping concentration and barrier height values are also estimated from the $C−V$ measurements and the corresponding values are 0.62 V, 1.20×10^{17} cm^{-3} and 0.79 eV, respectively. The interface state density (N_{SS}) obtained from forward bias $I−V$ characteristics by considering the series resistance (R_S) values are lower without considering the series resistance (R_S). Furthermore, the interface state density (N_{SS}) and relaxation time (τ) are also calculated from the experimental $C−f$ and $G−f$ measurements. The N_{SS} values obtained from the $I−V$ characteristics are almost three orders higher than the N_{SS} values obtained from the $C−f$ and $G−f$ measurements. The experimental results depict that N_{SS} and τ are decreased with bias voltage. The frequency dependence of the series resistance (R_S) is attributed to the particular distribution density of interface states.

1. Introduction

In recent years, the nitride-based materials have attracted much attention due to their high thermal conductivity, higher electron mobility, higher electron saturation velocity, and large band gap. The nitride-based semiconductors such as GaN, AlGaN, AlInN, InGaN, and AlGaInN alloys are very appropriate for the production of visible-light-emitting diodes (LEDs) covering the entire violet, blue, and bluish-green region and are capable for short-wavelength laser diodes (LD) due to their wide and direct-energy band gap [1–4]. Due to the tunability of the band gap for InGaN from infrared to ultraviolet $(0.7−3.4\,\text{eV})$ [5] by adjusting their In/Ga ratio, it has been widely used in various optoelectronic and energy applications [6]. However, it is very difficult to produce high quality Schottky contacts to InGaN, because InGaN with a high indium concentration will have low carrier mobility and also have large surface defects. For that reason, it is very important to fabricate Schottky contacts on n-type InGaN that have good thermal stability and large Schottky barriers in the realization of optoelectronic devices.

Many researchers have investigated the optical properties of InGaN based structures. However, there are only limited works on the electrical and structural properties of InGaN Schottky barrier diodes (SBDs). For example, Sang et al. [7] investigated the thermally stable high performance InGaN metal-insulator-semiconductor (MIS) Schottky-type photodiode by using CaF$_2$ as an insulating layer. The temperature dependent current-voltage $(I−V)$ characteristics were analysed by using the thermionic-field emission (TFE) and field emission (FE) tunnelling mechanisms from room temperature to 463 K and concluded that TFE is the dominant mechanism at high temperatures. Arslan et al. [8]

fabricated the Pt/p-InGaN and Pt/n-InGaN Schottky barriers in a wide temperature range $(80−360\,\text{K})$. They reported that the dominant current transport across the Pt/n-InGaN and Pt/p-InGaN Schottky diodes are the electron tunnelling to deep levels in the vicinity of mixed or screw dislocations in the temperature range of $80−360\,\text{K}$. Padma et al. [6] investigated the electrical and structural properties of Ir/Ru Schottky contacts on n-InGaN at different annealing temperatures. They demonstrated that the 300°C was the optimum annealing temperature and also reported that the Ga−Ir interfacial phases were responsible to increase the barrier height at 300°C. Padma et al. [9] investigated the capacitance-frequency $(C−f)$ and conductance-frequency $(G−f)$ characteristics of Ir/n-InGaN Schottky diodes with various biases and at different temperatures. They showed that, at low frequencies, the higher values of capacitance are due to the excess capacitance resulting from the interface states in equilibrium with the semiconductor (n-InGaN) that could follow the alternating current (ac) signal.

Tuan et al. [10] fabricated the Pt/SiO$_2$/n-InGaN metal-oxide-semiconductor (MOS) diodes by RF sputtering and investigated the electrical properties of as-deposited and 400°C annealed contacts by current-voltage $(I−V)$ and capacitance-voltage $(C−V)$ measurements. They obtained the higher barrier height, lower leakage current and better ideality factor for 400°C annealed contact compared to the as-deposited contact. Asghar et al. [11] investigated the $I−V$ measurements of commercially available InGaN based blue light emitting diode (LED) at different temperatures $(305−170\,\text{K})$ by deep level transient spectroscopy (DLTS) technique. They demonstrated that the barrier height values were decreased with decrease in temperature and the ideality factor values were increased with decrease in

temperature. Also they reported that the higher ideality factor values are due to the high diffusion or tunnelling currents.

In our previous work, the detailed electrical and structural properties of Ir/Ru/n-InGaN Schottky barrier diodes were investigated at different annealing temperatures. The capacitance-frequency $(C-f)$ and conductance-frequency $(G-f)$ measurements furnish the substantial information about the interface state density distribution profiles and relaxation time of the diode. Therefore, the main focus of this work is to characterize the capacitance-frequency $(C-f)$, conductance-frequency $(G-f)$ and series resistance-frequency (R_S-f) measurements and analyse the density distribution and relaxation time of the interface states for the Ir/Ru/n-InGaN Schottky diodes at room temperature.

2. Experimental details

The samples used in the work were $2\,\mu$m-thick unintentionally doped GaN layer on a $40\,$nm-thick nucleation layer/(0001) sapphire substrate was grown by metal organic chemical vapour deposition (MOCVD), which was followed by the growth of $0.25\,\mu$m-thick n-InGaN:Si ($N_d = 7 \cdot 10^{17}\,$cm^{-3}) with 10% of indium composition. Prior to the metal deposition the n-InGaN samples were ultrasonically degreased with warm organic solvents like trichloroethylene followed by methanol and ethanol for 5 min in each step and then the samples were rinsed with deionized (DI) water. To remove the surface oxides, the degreased layer was dipped into boiling aquaregia [HNO$_3$:HCl=1:3] for 10 min and then rinsed with DI water. For ohmic contacts, Ti/Al (25/100 nm) layers were deposited on a portion of the sample by electron beam evaporation technique under a pressure of $5 \cdot 10^{-6}$mbar. Then the samples were annealed at $650°$C for 1 min in nitrogen (N$_2$) ambient using rapid thermal annealing (RTA) system. Finally, for Schottky contacts, Ir/Ru (20/30 nm) were deposited on the other portion of the sample with 0.7 mm circular dots through stainless steel mask by electron beam evaporation system with a pressure of $5 \cdot 10^{-6}$ mbar. The schematic diagram of the Ir/Ru/n-InGaN SBD was shown in Fig. 1. The current-voltage $(I-V)$ and capacitance-voltage $(C-V)$ characteristics were measured by a Keithley source measurement unit (Model no: 2400) and automated deep level transient spectrometer (DLS-83D). The capacitance-frequency $(C-f)$ and conductance-frequency $(G-f)$ characteristics have been measured using a phase sensitive multimeter (PSM 1700) at room temperature with different biases.

3. Results and dicussion

The forward and reverse semi-logarithmic current-voltage $(I-V)$ characteristics of Ir/Ru/n-InGaN Schottky barrier diode (SBD) at room temperature is shown in Fig. 2. The
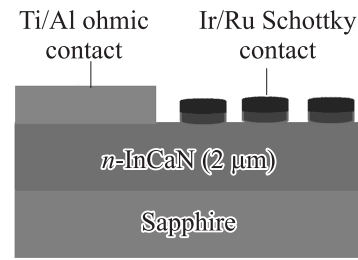

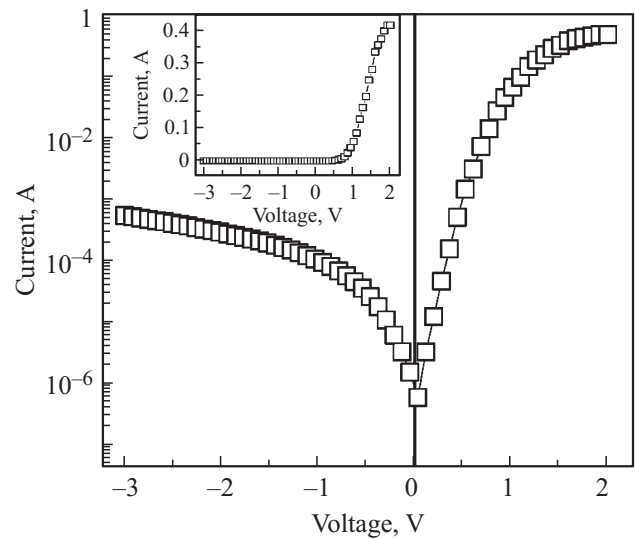**Figure 1.** Schematic diagram of the Ir/Ru/n-InGaN SBD.

Figure 2. Forward and reverse bias current-voltage $(I-V)$ characteristics of the Ir/Ru/n-InGaN SBD at room temperature. The inset shows the linear $I-V$ characteristics of the diode.
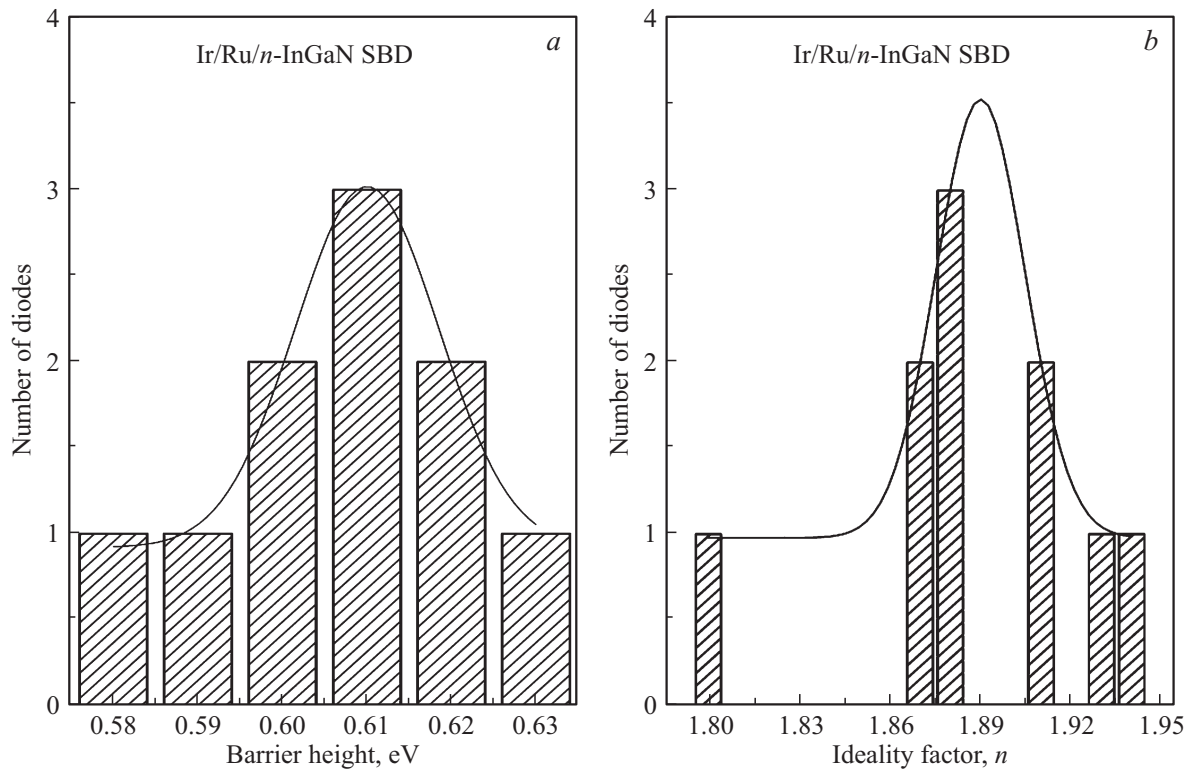
linear $I-V$ characteristic of the Ir/Ru/n-InGaN SBD is also shown in the inset of Fig. 2. Clearly, it is observed from the Fig. 2, that the diode shows good rectifying behaviour [12]. The measured leakage current of the Ir/Ru/n-InGaN SBD is $1.003 \cdot 10^{-4}$ A at -1 V. The $I-V$ characteristics of the SBD can be analyzed by thermionic emission (TE) theory. The relation between the current and applied forward voltage $(V > 3kT/q)$ can be expressed as [12,13]

$$I = I_0 \exp\left(\frac{q(V - IR_S)}{nkT}\right)\left[1 - \exp\left(-\frac{q(V - IR_S)}{kT}\right)\right],\tag{1}$$

where q is the charge of electron, n is the ideality factor, k is the Boltzmann constant, V is the applied bias voltage, T is the absolute temperature in Kelvin and the term IR_S is the voltage drop across the series resistance (R_S). The reverse saturation current (I_0) can be determined from the intercept of the linear region of the $\ln I-V$ plot at zero bias and it can be expressed as

$$I_0 = AA^*T^2 \exp\left(\frac{-q\Phi_{b0}}{kT}\right),\tag{2}$$

where A^* is the Richardson constant (23 A/cm^{2}K^2 for n-type InGaN), A is the diode area and Φ_{b0} is the zero-bias barrier

Figure 3. Gaussian distribution of the barrier heights and ideality factors estimated from forward bias $I-V$ characteristics of Ir/Ru/n-InGaN SBD.

height which can be calculated from Eq. (2). One of the other important parameters is the ideality factor n, which can be evaluated from the slope of the linear region of the $\ln I - V$ plot and can be expressed as follows

$$ n = \frac{q}{kT}\left(\frac{dV}{d(\ln I)}\right). \qquad (3) $$

Ten Ir/Ru/n-InGaN Schottky barrier diodes (SBDs) are fabricated and measured $I-V$ characteristics for each diode at room temperature. Results showed that the barrier height (BHs) of Ir/Ru/n-InGaN SBDs varied in the range from 0.58 to 0.63 eV, and ideality factor values range from 1.8 to 1.94. Fig. 3, a and b show the statistical distribution of the BHs and ideality factors for the Ir/Ru/n-InGaN SBD estimated from the $I-V$ characteristics. The experimental distributions of the BHs and ideality factor values are fitted by the Gaussian function. The statistical analysis of the diodes has yielded a mean BH value of 0.61 eV with a standard deviation of 0.017 eV, and mean ideality factor value of 1.89 with a standard deviation of 0.029. The ideality factor mentioned is estimated in the voltage range 0.032 to 0.524 V. Usually $n = 1$ for ideal diode, so the high value of ideality factor can be attributed to the effect of series resistance, voltage dependence of the BH and the voltage drop across the interfacial layer. Such type of interfacial layer is formed while fabricating the device by using conventional methods and before the process of the evaporation of the metals on the front surface of the n-type InGaN substrate [14–16].

The series resistance (R_S) and shunt resistance (R_{sh}) are also other important parameters which are influenced on the diode characteristics. The values of R_S and R_{sh} are determined from the plot of diode junction resistance (R_J) versus applied voltage as shown in Fig. 4, where $R_J = \partial V/\partial I$ which have been extracted from the $I-V$ characteristics. For ideal diodes the series resistance as low as zero, ensures that high current will flow through the device whereas shunt resistance reaching to infinity, indicates small leakage current
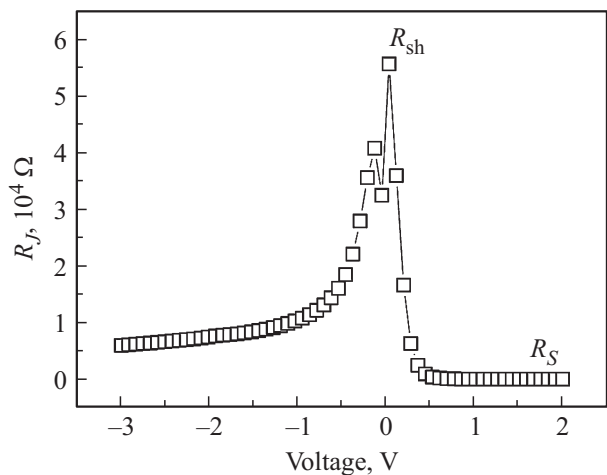
Figure 4. Plot of junction resistance for the Ir/Ru/n-InGaN SBD at room temperature.

in the device. It is observed that the junction resistance approaches to a constant value at higher voltages in the forward bias and this value is taken as R_S, while in the reverse bias the maximum value of the junction resistance is equal to the diode R_{sh}. From Fig. 4, the values of R_S and R_{sh} are found to be $4.80\,\Omega$ and $55.87\,k\Omega$ for the Ir/Ru/n-InGaN SBD, respectively.

The capacitance-voltage $(C-V)$ measurement has a significant importance for the SBDs. In the case of reverse bias voltage, the dependence of capacitance on the voltage could be given some diode parameters such as diffusion or built-in potential, carrier concentration and BH of the device. The capacitance of the depletion region under a reverse bias in the metal-semiconductor (MS) contacts and it can be expressed [17] as

$$\frac{1}{C^2} = \frac{2(V_{bi} - V)}{A^2 \varepsilon_s \varepsilon_0 q N_d}, \quad (4)$$

where A is the diode area, ε_s is the dielectric constant of the semiconductor ($\varepsilon_s = 8.4\varepsilon_0$), ε_0 is the dielectric constant of the vacuum, N_d is the donar concentration, V is the applied bias voltage and V_{bi} is the built in potential which could be calculated from the extrapolation of the linear part of the $1/C^2-V$ plot to the x-$axis$. The barrier height Φ_{b0} can be deduced by the following relation,

$$\Phi_{b0(C-V)} = V_{bi} + V_n, \quad (5)$$

where V_n is the potential difference between the Fermi energy level and the bottom of the conduction band in the neutral part of the semiconductor (n-InGaN) and it can be given as

$$V_n = \frac{kT}{q} \ln\left(\frac{N_C}{N_d}\right), \quad (6)$$

where N_C is the density of the states in the conduction band edge and is given by $N_C = 2(2\pi m^* kT/h^2)^{3/2}$, $m^* = 0.19 m_0$ and its value was $7 \cdot 10^{17}\,cm^{-3}$ for InGaN at room temperature. The plot of $1/C^2-V$ curves at room temperature for the Ir/Ru/n-InGaN SBD at 1 MHz frequency is shown in Fig. 5. The inset of Fig. 5 shows the capacitance-voltage curve of the Ir/Ru/n-InGaN SBD at room temperature. From Fig. 5, the built-in potential, carrier concentration and BHs the Ir/Ru/n-InGaN SBD are found to be 0.62 V, $1.20 \cdot 10^{17}\,cm^{-3}$ and 0.79 eV. The BH extracted from the $C-V$ measurements is higher than the BH obtained from $I-V$ measurements. These results may be expected for no$n$-ideal Schottky diodes. This discrepancy can be explained due to the excess capacitance and the interfacial layer or barrier inhomogenities [17]. Such differences in the BHs determined from the $I-V$ and $C-V$ measurements are caused by the existence of the spatial inhomogenities at the metal-semiconductor (MS) interface of abrupt Schottky contacts suggested by Werner and Guttler [18]. Another reason may be the inhomogeneities affect on apparent BH since current across interface depends exponentially on BH and the current is sensitive to barrier distribution at the
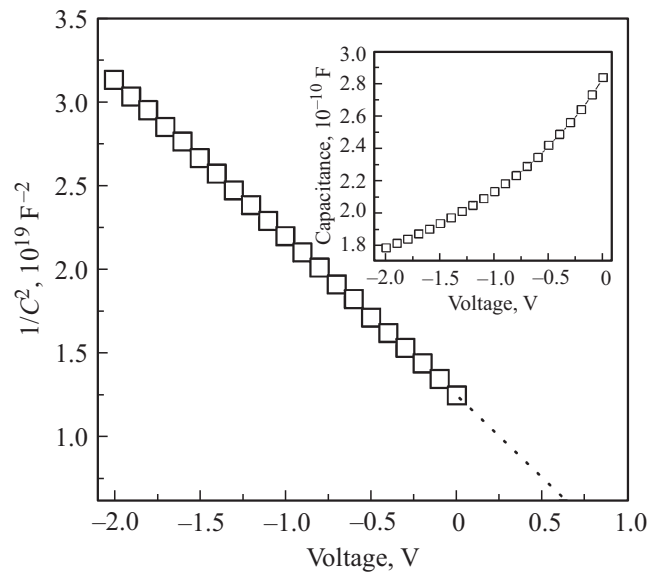
Figure 5. Plot of $1/C^2$ versus V for the Ir/Ru/n-InGaN SBD at room temperature. The inset shows the capacitance-voltage $(C-V)$ curve of the diode.

interface. The BH estimated from $C-V$ method includes an average value of BHs of patches existing in the contact [19].

The interface state density (N_{SS}) plays an important role for the understanding of the electrical properties of rectifying MS structures. The energy distribution profiles of N_{SS} are also determined from the forward bias $I-V$ characteristics, by taking into the effective BH (Φ_e) and the voltage dependent ideality factor $(n(V))$. The quantities of $n(V)$ and Φ_e can be expressed by the following equations, respectively [20]

$$n(V) = \frac{q}{kT} \left[\frac{V - IR_S}{\ln(I/I_0)}\right], \quad (7)$$

$$\Phi_e = \Phi_{b0} + \beta(V - IR_S) = \Phi_{b0} + \left(1 - \frac{1}{n(V)}\right)(V - IR_S), \quad (8)$$

where $\beta[= d\Phi_e/dV = 1 - 1/n(V)]$ is the voltage coefficient of the effective BH (Φ_e) used in the place of zero-bias BH Φ_{b0} [20]. For Schottky diodes having interface states in equilibrium with the semiconductor, the ideality factor n becomes greater than unity as proposed by Card and Rhoderick [20] and is given by the relation

$$n(V) = 1 + \frac{\delta}{\varepsilon_1}\left[\frac{\varepsilon_s}{W_D} + qN_{SS}\right]. \quad (9)$$

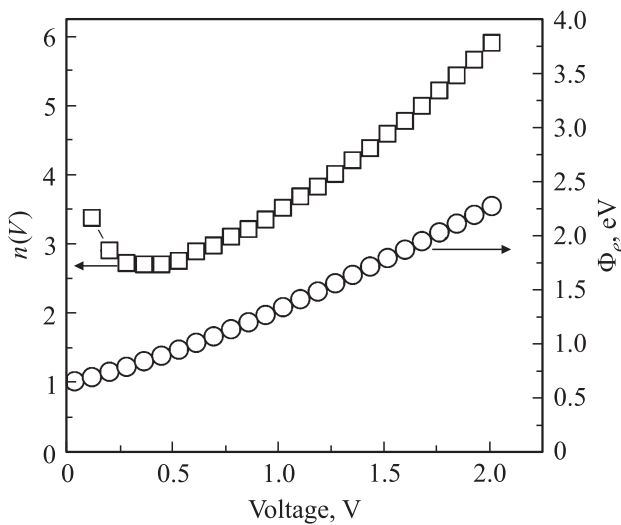The expression for interface state density (N_{SS}) as determined by Card and Schroder [21,22] is reduced to

$$N_{SS} = \frac{1}{q}\left[\frac{\varepsilon_i}{\delta}\left(n(V) - 1\right) - \frac{\varepsilon_s}{W_D}\right], \quad (10)$$

where ε_i and ε_s are the permittivity of the interfacial layer and semiconductor, respectively. δ is the thickness of the

interfacial layer and W_D is the width of the depletion layer, which are calculated from the reverse bias $C-V$ characteristics at 1 MHz. Furthermore, for n-type semiconductors, the energy of interface states E_{SS} with reference to the bottom of the conduction band edge E_C, at the surface of the semiconductor is given by [20]
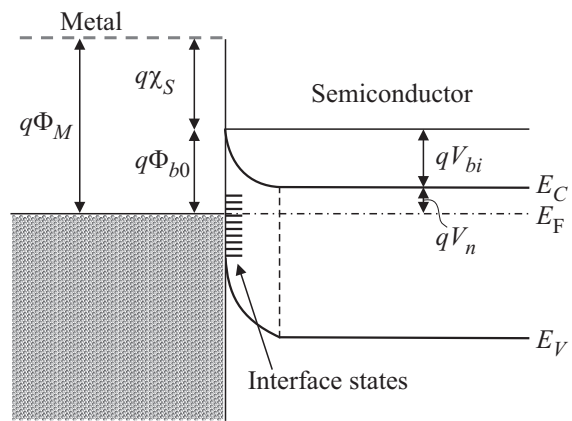
$$E_C - E_{SS} = q(\Phi_e - V). \tag{11}$$

Fig. 6 shows the plot of voltage dependent ideality factor $(n(V))$ and effective BH (Φ_e) as function of applied forward bias voltage. As can be seen from the Fig. 6 both are voltage dependent, which may be due to the presence of

Figure 8. The energy level band diagram of the Ir/Ru/n-InGaN SBD with interface states at room temperature: where Φ_M is the metal work function, Φ_{b0} is the barrier height, χ_S is the semiconductor electron affinity, V_n is the potential difference between the Fermi level and conduction band and V_{bi} is the built-in potential, respectively.

Figure 6. The voltage dependent ideality factor $n(V)$ and effective barrier height (Φ_e) versus applied forward bias voltage for Ir/Ru/n-InGaN SBD at room temperature.
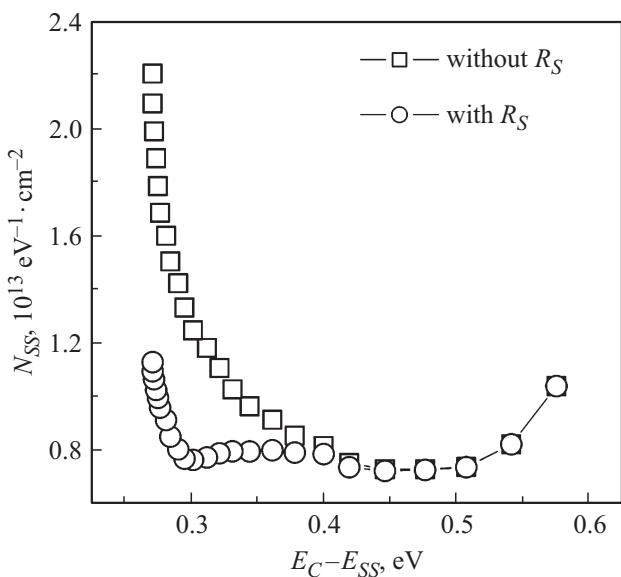
Figure 7. The interface state density distribution (N_{SS}) as a function of $E_C - E_{SS}$ for the Ir/Ru/n-InGaN SBD at room temperature.

native interfacial insulator layer and interface states located between the interfacial layer and the semiconductor [23]. The plot of N_{SS} with and without considering the series resistance (R_S) as a function of $E_C - E_{SS}$ by Eqs (10) and (11) at room temperature is shown in Fig. 7. From Fig. 7, it is clear that the exponential growth of the N_{SS} towards the bottom of the conduction band is very apparent, which indicates the continuum of the interface states. The magnitude of N_{SS} for the Ir/Ru/n-InGaN SBDs without and with taking into account the R_S are in the range from $2.19 \cdot 10^{13}$ to $1.03 \cdot 10^{13}$ eV^{-1}cm^{-2} and from $1.12 \cdot 10^{13}$ to $1.03 \cdot 10^{13}$ eV^{-1}cm^{-2} at $(E_C - 0.27)$ to $(E_C - 0.57)$ eV, respectively. From the above experimental results, it is noted that the N_{SS} values with considering the R_S values are lower than that of without considering the R_S. These results clearly demonstrated that the R_S value is very important and must be taken while calculating the density distribution profiles of N_{SS}. Fig. 8 shows the energy level band diagram of the Ir/Ru/n-InGaN SBD with an interface states at room temperature.

Fig. 9 shows the measured capacitance-frequency $(C-f)$ characteristics of the Ir/Ru/n-InGaN SBD at room temperature at different biases from 0.0 to 0.5 V with steps of 0.1 V. From Fig. 9, it is clearly seen that, the capacitance decreases with increase in the frequency and reached to a constant value. The higher value of capacitance at lower frequencies is due to the excess capacitance consequential from the interface states in equilibrium with the n-InGaN that can follow the alternating current signal. Whereas, at higher frequencies the capacitance is not dispersive and thus, the interface state in equilibrium with the n-InGaN do not contribute to the capacitance, because the charges at the interface states cannot follow the alternating current signal. Therefore at lower frequencies, the total capacitance is equal to the sum of the space charge capacitance and
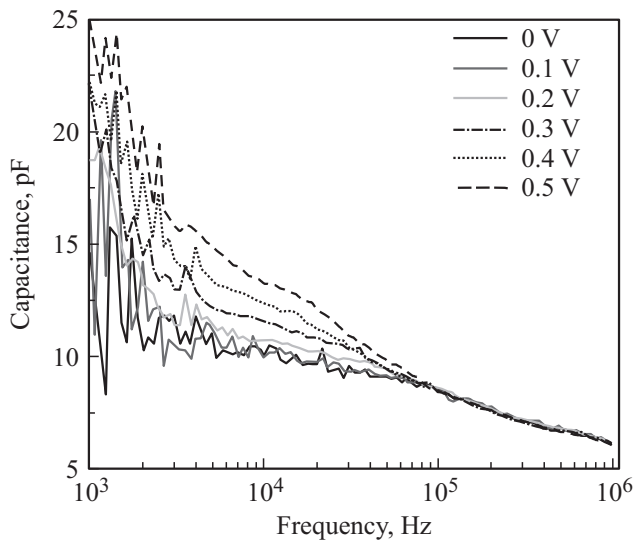
Figure 9. Experimental $C-f$ characteristics of the Ir/Ru/n-InGaN SBD with various biases (0.0−0.5 V with steps of 0.1 V) at room temperature.
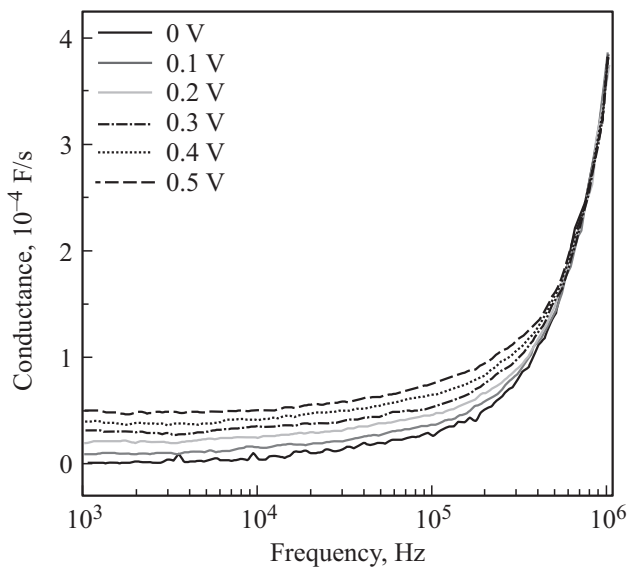
Figure 10. Experimental $G-f$ characteristics of the Ir/Ru/n-InGaN SBD with various biases (0.0−0.5 V with steps of 0.1 V) at room temperature.

excess capacitance, while at higher frequencies the total capacitance is due to almost only from the space charge capacitance [24,25]. It means that at higher frequencies, the interface state capacitance does not make any contribution to the total capacitance. The experimental conductance-frequency ($G-f$) characteristics of the Ir/Ru/n-InGaN SBD (0.0−0.5 V with steps of 0.1 V) at room temperature is shown in Fig. 10. As can be seen from Fig. 10, at lower frequency scale the experimental conductance value is almost constant up to a certain frequency value. Further, if the frequency increases the conductance continuously increased for all the applied voltages.

It is also possible to calculate the density distribution of the interface states from experimental capacitance-frequency ($C-f$) and conductance-frequency ($G-f$) characteristics of the Ir/Ru/n-InGaN SBD at room temperature. The interface state conductance (G_{SS}) can be deduced by Nicollian and Goetzberger [26] is given as

$$G_{SS} = \frac{AqN_{SS}}{2\tau} \ln(1 + \omega^2\tau^2), \qquad (12)$$

where $\omega(= 2\pi f)$ is the angular frequency and τ is the time constant of the interface states which can be written by the following equation

$$\tau = \frac{1}{v_{th}\sigma N_d} \exp\left(\frac{qv_d}{kT}\right), \qquad (13)$$

where A is the diode area, N_{SS} is the interface state density, σ is the capture cross-section of the interface states, V_{th} is the thermal velocity of the carrier, N_d is the doping concentration, k is the Boltzmann constant, T is the temperature in Kelvin and τ is the relaxation time of the interface states.
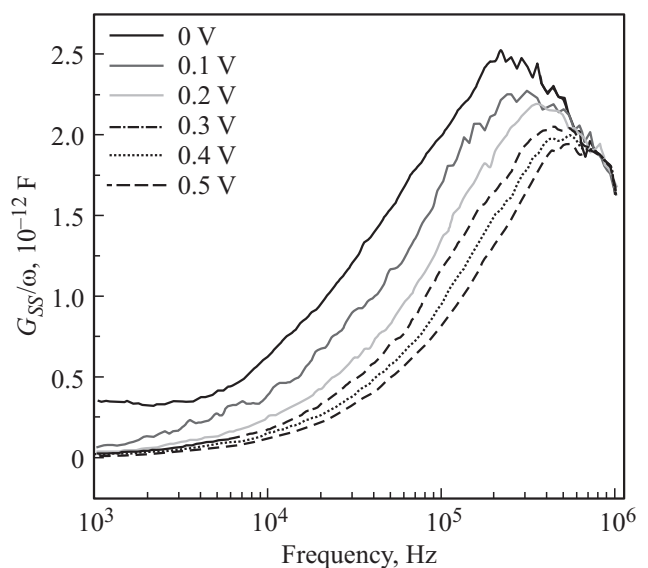
The conductance of the interface states G_{SS} is given by the relation [27,28]

$$G_{SS} = \frac{C_{ox}^2 G}{(C_{ox} - C)^2 + (G/\omega)^2}. \qquad (14)$$

Furthermore, in n-type semiconductor the density of states E_{SS} with respect to the bottom of the conduction band is given by

$$E_C - E_{SS} = q\Phi_b - qV. \qquad (15)$$

In order to determine the interface state density of the Ir/Ru/n-InGaN SBD at room temperature the curves of

Figure 11. G_{SS}/ω versus frequency characteristics of the Ir/Ru/n-InGaN SBD depending on the bias voltage (0.0−0.5 V with steps of 0.1 V) at room temperature.

G_{SS}/ω versus $\log(f)$ are plotted and is shown in Fig. 11. From Fig. 11, it is noted that a peak is observed in the curves and the peak position shifts from lower frequency to higher frequency with the applied bias. The presence of peak confirms the existence of the interface traps. The maxima of the G_{SS}/ω plot (Fig. 11) will give the interface state density (N_{SS}) and relaxation (τ) time. The curves go through maximum at $\omega\tau = 1.98$ with the value of $(G_{SS}/\omega)_{max} = 0.40AqN_{SS}$ [26,27]. The dependence of interface state density and relaxation times are converted as a function of E_{SS} by using Eq. (15). The energy distribution profiles of the interface states and their relaxation times are obtained from G_{SS}/ω versus f plot of the Ir/Ru/n-InGaN SBD at room temperature as a function of $E_C - E_{SS}$ are shown in Fig. 12. The magnitude of interface state density and relaxation times are in the range of $1.02 \cdot 10^{10}\,\mathrm{eV}^{-1}\mathrm{cm}^{-2}$ and $1.45 \cdot 10^{-6}\,\mathrm{s}$ in $(E_C - 0.61)\,\mathrm{eV}$ to $7.91 \cdot 10^9\,\mathrm{eV}^{-1}\mathrm{cm}^{-2}$ and $5.89 \cdot 10^{-7}\,\mathrm{s}$ in $(E_C - 0.11)\,\mathrm{eV}$, respectively. Both the interface state density and relaxation times slightly rise from the mid gap to the bottom of the conduction band.

Furthermore, the interface state density curves obtained from the $C-f$ and $G-f$ characteristics (Fig. 12) are compared with the interface state density extracted from the forward bias $I-V$ characteristics (Fig. 7). As can be seen clearly from Figs. 7 and 12, the interface state density obtained from the $C-f$ and $G-f$ characteristics are much smaller than that are obtained from the forward bias $I-V$ characteristics. This difference is almost three orders in the magnitude. These results are more consistent with the results achieved by Victorovitch et al. [29] and Ayyildiz et al. [30]. Based on the explanation reported in references [29,30], the large differences between the interface state density values obtained from the $C-f$,

]
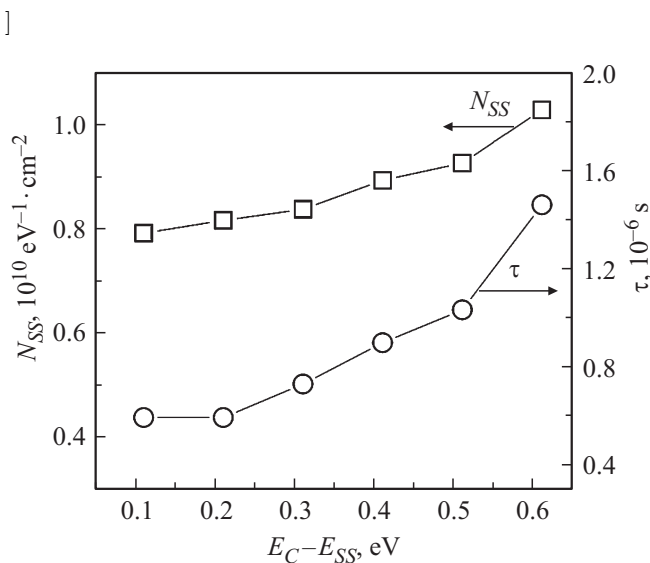
Figure 12. The variation of interface state density (N_{SS}) and relaxation time (τ) as a function of $E_C - E_{SS}$ for the Ir/Ru/n-InGaN SBD at room temperature.
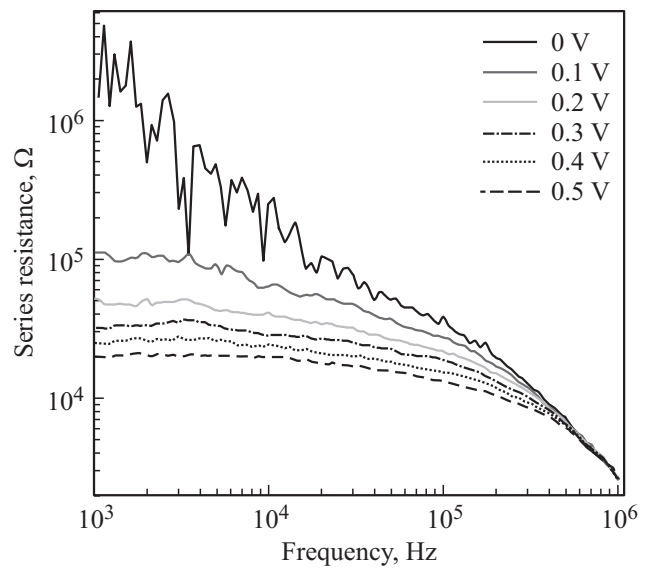
Figure 13. $R_S - f$ characteristics of the Ir/Ru/n-InGaN SBD with various biases $(0.0-0.5\,\mathrm{V}$ with steps of $0.1\,\mathrm{V})$ at room temperature.

$G-f$ and $I-V$ characteristics may be due to the local trap-density effect at the oxide-semiconductor interface. The traps are effectively concentrated across the current parts; $I-V$ characteristics provide the determination of the local density of traps in the areas crossed by the current. Hence, the average density of traps determined from admittance measurements can be significantly lower than the local density [29,30] (by about three orders of magnitude).

The other important parameter for the Schottky devices is series resistance (R_S). The frequency dependence of the series resistance for the Ir/Ru/n-InGaN SBD at room temperature at different biases is shown in Fig. 13. The series resistance for the diode can be evaluated from the $C-V-f$ measurements as

$$R_S = \frac{G}{G^2 + (\omega C)^2}, \qquad (16)$$

where C and G are the measured capacitance and conductance values. The series resistance of the Ir/Ru/n-InGaN SBD can be calculated by Eq. (16). From Fig. 13, it is observed that the series resistance is almost constant at lower frequencies and decreases at higher frequencies. The frequency dependence of series resistance is attributed to the particular distribution density of interface states [31].

4. Conclusions

The electrical properties of a fabricated Ir/Ru/n-InGaN SBD have been investigated by $I-V$, $C-V$, $C-f$ and $G-f$ characteristics at room temperature. The Ir/Ru/n-InGaN SBD shows good rectifying behaviour. The mean barrier height (BH) and ideality factors are found to be $0.61\,\mathrm{eV}$ and 1.89, respectively. Also, the BH is calculated from

$C−V$ method and value is 0.79 eV. The discrepancy between the BHs obtained from $I−V$ and $C−V$ is also discussed. Furthermore, the interface state density (N_{SS}) is also determined from the forward bias $I−V$ characteristics with and without taking into account the R_S. The measured capacitance decreases with increasing the frequency. At lower frequencies higher values of capacitance are due to the excess capacitance resulting from the interface states that can follow the alternating current signal. Moreover, the energy distribution profiles of the interface states and their relaxation times are also evaluated from $C−f$ and $G−f$ measurements. The N_{SS} values determined from $C−f$ and $G−f$ are much smaller than the N_{SS} values determined from the forward bias $I−V$ characteristics. The N_{SS} and τ values slightly rise from the mid gap towards the bottom of the conduction band.

References

[1] S. Nakamura, S. Pearton, G. Faso. *The Blue Laser Diode* (Springer-Verlag, The complete story, 2000).

[2] H. C. Casey, J. Muth, S. Krishnankutty. J.M. Zavada, Appl. Phys. Lett., **68**, 2867 (1996).

[3] Z.L. Li, P.T. Lai, H.W. Choi. IEEE Phot. Techn. Lett., **21**, 1429 (2009).

[4] X.A. Cao, E.B. Stokes, P.M. Sandvik, S.F. LeBoeuf, J. Kretchmer, D. Walker. IEEE Electron. Dev. Lett., **23**, 535 (2002).

[5] S. H. Abud, Z. Hassan, F. Yam. Int. J. Electrochem. Sci., **7**, 10038 (2012).

[6] R. Padma, B. Prasanna Lakshmi, M. Siva Pratap Reddy, V. Rajagopal Reddy. Superlat. Microstruct., **56**, 64 (2013).

[7] L. Sang, M. Liao, Y. Koide, M. Sumiya. Appl. Phys. Lett., **99**, 031115 (1) (2011).

[8] E. Arslan, H. Cakmak, E. Ozbay. Microelectron. Eng., **100**, 51 (2012).

[9] R. Padma, B. Prasanna Lakshmi, V. Rajagopal Reddy. Superlat. Microstruct., **60**, 358 (2013).

[10] T.T.A. Tuan D.-H. Kuo. Mat. Sci. Semicond. Process., **30**, 314 (2015).

[11] H.M.N.H.K. Asghar, Z.A. Gilani, M.S. Awan, I. Ahmad, Y. Tan. Arab. J. Sci. Eng., **40**, 263 (2015).

[12] S.M. Sze. *Physics of Semiconductor Devices* (Wiley, N.Y., 1979).

[13] E.H. Rhoderick, R.H. Williams. *Metal-Semiconductor Contacts* (Clarendon, Oxford, 1988).

[14] F. Yakuphanoglu, M. Kandaz, B. Senkal. Thin Solid Films, **516**, 8793 (2008).

[15] W. Monch. *Semiconductor Surfaces and Interfaces*, 3rd ed. (Springer, Berlin, 2001).

[16] S. Karatas, S. Altindal. Mater. Sci. Eng. B, **122**, 133 (2005).

[17] C. Coskun, S. Aydogan, H. Efeoglu. Semicond. Sci. Technol., **19**, 242 (2004).

[18] J.H. Werner, H.H. Guttler. J. Appl. Phys., **69**, 1522 (1991).

[19] A. Tataroglu, S. Altindal. Microelectron. Eng., **83**, 582 (2006).

[20] H.C. Card, E.H. Rhoderick. J. Phys. D: Appl. Phys., **4**, 1589 (1971).

[21] R. Hackam, P. Harrop. IEEE Trans. Electron. Dev., **9 (12)**, 1231 (1972).

[22] D.K. Schroder. *Semiconductor Material Device Characterization* (Wiley, London, 1998).

[23] M.A. Kadaoui, W.B. Bouiadjra, A.Saidane, S. Belahsene. Superlat. Microstruct., **82**, 269 (2015).

[24] A.F. Ozdemir, A. Gok, A. Turut. Thin Solid Films, **515**, 7253 (2007).

[25] A. Turut, N. Yalcin, M. Saglam. Sol. St. Electron., **35**, 835 (1992).

[26] E.H. Nicollian, A. Goetzberger. Bell Syst. Tech. J., **46**, 1055 (1967).

[27] E.H. Nicollian, J.R. Brews. *MOS (Metal Oxide Semiconductor) Physics Technology* (John Wiley and Sons, N.Y., 1982).

[28] J. Fernandez, P. Godignon, S. Berberich, J. Rebollo, G. Brezenanu. Sol. St. Electron., **39**, 1359 (1996).

[29] P. Victorovitch, P. Louis, M.P. Besland, A. Chovet. Sol. St. Electron., **38**, 1035 (1995).

[30] E. Ayyildiz, C. Nuho Lu, A. Turut. J. Electon. Mater., **31**, 119 (2002).

[31] F. Parlaktuk, A. Altindal, A. Tataroglu, M. Partakm, A. Agasier. Microelectron. Eng., **85**, 81 (2008).